# Carrier transport via V-shaped pits in InGaN/GaN MQW solar cells*

Shitao Liu(刘诗涛)[1], Zhijue Quan(全知觉)[2], and Li Wang(王立)[1,†]

[1] School of Materials Science and Engineering, Nanchang University, Nanchang 330031, China
[2] National Engineering Technology Research Center for LED on Si Substrate, Nanchang University, Nanchang 330047, China

(Received 19 September 2016; revised manuscript received 23 November 2016; published online 13 February 2017)

Carrier transport via the V-shaped pits (V-pits) in InGaN/GaN multiple-quantum-well (MQW) solar cells is numerically investigated. By simulations, it is found that the V-pits can act as effective escape paths for the photo-generated carriers. Due to the thin barrier thickness and low indium composition of the MQW on V-pit sidewall, the carriers entered the sidewall QWs can easily escape and contribute to the photocurrent. This forms a parallel escape route for the carries generated in the flat quantum wells. As the barrier thickness of the flat MQW increases, more carriers would transport via the V-pits. Furthermore, it is found that the V-pits may reduce the recombination losses of carriers due to their screening effect to the dislocations. These discoveries are not only helpful for understanding the carrier transport mechanism in the InGaN/GaN MQW, but also important in design of the structure of solar cells.

**Keywords:** V-shaped pits, InGaN/GaN multiple-quantum-well, solar cells, carrier transport

**PACS:** 81.07.St, 81.05.Ea, 88.40.jm **DOI:** 10.1088/1674-1056/26/3/038104

## 1. Introduction

Due to its tunable band gap from 3.4 eV to 0.65 eV, InGaN alloy is a promising material for high efficiency multi-junction solar cell.[1] However, the large lattice mismatch between GaN and InN makes it extremely difficult to grow thick high quality InGaN film with sufficient indium composition.[2] It is reported that the critical thickness of InGaN layer with 20% indium composition on GaN is less than 6 nm,[3] which is far from enough for solar cells. Owing to the intensive study of blue LED, growth process of high quality InGaN/GaN multiple quantum wells (MQW) has been well established, which makes it possible to obtain high quality InGaN layer with total thickness far beyond its critical thickness. Using the structure similar to LEDs, InGaN/GaN MQW solar cells have gained improvements in performances, and as compared to the traditional structure using thick single InGaN absorption layer, they have been demonstrated by several groups.[4–14] Because the carriers generated in the QWs would be confined by the quantum barriers (QBs), the amount of photocurrent is directly related to the escape probability of the carriers from the QWs. Therefore, understanding the carrier transport mechanism in the InGaN/GaN MQW is of great importance for design and fabrication of high performance solar cells.

Several studies regarding the carrier escape mechanism in InGaN MQW have been published in the literature.[8,15] In these studies, the carrier escape probability has been quantitatively discussed with the theoretical models considering the competition of carrier recombination, tunneling and thermionic emission. In these studies the MQWs were assumed to have ideal structure with perfect interfaces. However, it is well known that the InGaN/GaN MQWs are usually highly defective and have imperfect interfaces. It is found that some of the defects may not only affect the carrier recombination but also have a great influence on the carrier transport. For example, the commonly observed V-shaped pits (V-pits) in InGaN/GaN MQW have been revealed both theoretically and experimentally to play an important role in the carrier injection of LEDs.[16–19] Due to the similar structure of InGaN/GaN MQW solar cell to LED, it is therefore necessary to study the effect of the V-pits on the carrier transport in solar cells to obtain a better understanding of these devices. In this article, we present a simulation study on the effect of V-pits on carrier transport in the InGaN/GaN MQW solar cells. We will demonstrate that the V-pits can enhance carrier escape from the QWs and reduce carrier recombination losses by screening the dislocations. Our results indicate that manipulating the V-pits is a possible way to effectively improve the energy conversion efficiency of InGaN/GaN MQW solar cells.

## 2. Theoretical models and simulation parameters

The simulations were conducted using the ATLAS program,[20] which can solve the Poisson-Schrodinger equation self-consistently. The spontaneous and piezoelectric polarization models were considered for the built-in electric field. The polarization charge densities were calculated using the methods developed by Fiorentini and Bernardini.[21] Because the polarization charges could be partially screened by the free

*Project supported by the National Natural Science Foundation of China (Grant Nos. 61564007 and 11364034) and the Sci-Tech Support Plan of Jiangxi Province, China (Grant No. 20141BBE50035).

†Corresponding author. E-mail: wl@ncu.edu.cn

© 2017 Chinese Physical Society and IOP Publishing Ltd 

carriers or the defects, the polarization electric fields measured experimentally are usually weaker than those obtained by theoretical calculation.[22–24] For the sake of authenticity, a scale factor of 50% was used in our study for all the simulations. The carrier transport was calculated using the drift-diffusion model. The quantum effect was taken into account by applying the Bohm Quantum Potential model.[20]

To understand the effect of the V-pits in the InGaN/GaN MQW solar cells, we simulated both the structures with and without V-pits for a direct comparison. Figure 1 shows the schematic diagrams of the two structures, named as structure A and B, respectively. Figure 1(a) shows the cross sectional view of structure A. It consists of a 3-μm-thick n-GaN layer with electron concentration of $3\times10^{18}$ cm$^{-3}$, four periods of un-doped MQW with an indium composition of 0.2, and a 100-nm-thick p-GaN top layer with a hole concentration of $\sim3\times10^{17}$ cm$^{-3}$. The QW thickness of 3 nm is fixed in all the simulations while the barrier thickness varied from 3 nm to 15 nm. Figure 1(b) shows the cross sectional view of structure B. Flat regions of structure B and structure A are exactly the same. The wells and barriers at the center of Fig. 1(b) formed a V-shaped "pit". In a real InGaN/GaN MQW, the three-dimensional shape of a V-pit is an inverted pyramid with six sidewalls. For simplicity, here we use inverted cone to approximate the inverted pyramid because the former is easier to construct by the simulation program. The size of the device in Fig. 1(b) is 500 nm. The radius of the V-pit which intersects with the last quantum well is 14 nm. Thus, the V-pit accounts for about 0.3% of the whole device area and we assume the reduction of effective absorption area is negligible. The thicknesses of the sidewall MQW are set to be one third of those in the flat MQW, and the indium composition is set to be 5%.[16,25,26] It is pointed out that the difference in absorption efficiency for the two cells should be very small as illustrated in Fig. 1.

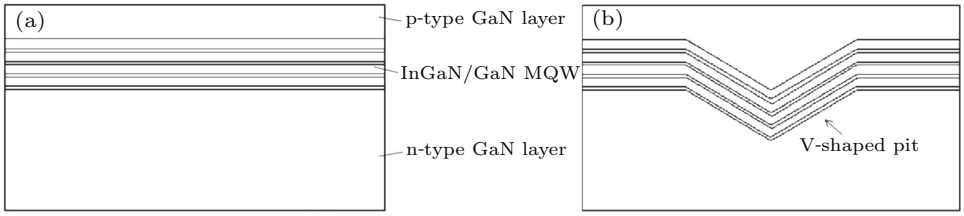



**Fig. 1.** Schematic diagrams of the InGaN/GaN solar cells with (a) or without V-pit (b).

**Table 1.** Parameters of GaN and InN used for simulation.

| Parameter | GaN | InN |
|---|---|---|
| Lattice constant/Å | 3.548 | 3.189 |
| Band gap $E_g$/eV | 3.42 | 0.65 |
| Dielectric constant $\varepsilon_s/\varepsilon_0$ | 8.9 | 10.5 |
| Electron mass $m_e/m_0$ | 0.2 | 0.05 |
| Hole mass $m_e/m_0$ | 1.25 | 0.6 |
| $\mu_e$/cm$^2\cdot$V$^{-1}\cdot$s$^{-1}$ | 350 | 350 |
| $\mu_h$/cm$^2\cdot$V$^{-1}\cdot$s$^{-1}$ | 3 | 3 |

The primary material parameters of GaN and InN used in the simulations are listed in Table 1.[27] For InGaN alloy, the parameters were calculated using the Vegard's Law. A bowing parameter of 1.43 was used for the calculation of band gap.[28] The band offset ratio of InGaN was set to be 60:40.[29] The radiative recombination, Shockley–Read–Hall (SRH) recombination and Auger recombination were all considered in the simulations. The threading dislocations were considered as non-radiative recombination centers (NRCs) and it is true that a V-pit always appears with a dislocation penetrating through its apex. To reflect this interaction, the dislocation was modeled as a cylinder penetrating the V-pit through its apex in present study. The radius of the cylinder is 0.6 nm. In the cylinder, a short SRH lifetime of 10 ps was set to reflect its nature of NRC. For all areas outside the cylinder, the SRH lifetime was set to be 100 ns.[24] The illumination employed in the simulations was the one sun AM1.5G solar spectrum. The wavelength-dependent absorption coefficients were calculated by[30]

$$\alpha(\lambda) = 2.2\times10^5\sqrt{\frac{1.24}{\lambda}-E_g}. \quad (1)$$

## 3. Simulation results and discussion

Table 2 shows the calculated performances of the two InGaN/GaN MQW solar cells depicted in Fig. 1. In both cells, the indium composition is 0.2 and the barrier thickness is 10 nm. These are typical parameters used in the previously reported studies for InGaN/GaN MQW solar cells. To manifest the role of the V-pit on carrier transport, here we did not take dislocation in the cells. Due to that the total thickness of the InGaN absorption layer is only 12 nm, the absolute conversion efficiencies of the two cells are low. However, the data given in Table 2 has clearly shown that the performance of structure B is superior to structure A. The open circuit voltages ($V_{oc}$) of the two cells are nearly equal. The short circuit current density ($J_{sc}$) and fill factor (FF) of structure B are 7.3% and 17.4% higher than structure A, respectively. Multiplying $V_{oc}$ by $J_{sc}$ and FF produces an efficiency increase of 26% for structure B, as compared to structure A.

**Table 1.** Simulated performances of InGaN/GaN MQW solar cells.

| Solar cell | Short circuit current density/mA·cm$^{-2}$ | Open circuit voltage/V | Fill factor/% | Conversion efficiency/% |
|---|---|---|---|---|
| without V-pit | 0.642 | 2.497 | 35.875 | 0.575 |
| with V-pit | 0.689 | 2.495 | 42.127 | 0.725 |

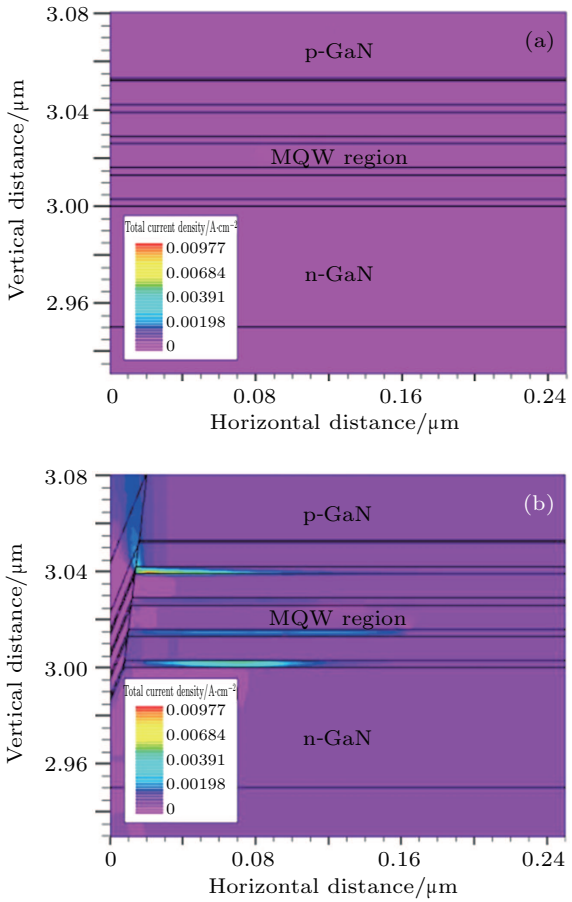



**Fig. 2.** (color online) Simulated contours of total current density for structure A (a) and structure B (b).

As mentioned before, the V-pit accounts for only 0.3% of the absorption area, which leads to a fact that it is not the carrier generation but the carrier collection responsible for the increase of the conversion efficiency. Figures 2(a) and 2(b) show the contours of total current density at zero bias for structure A and B, respectively. It is seen that the current density in structure A is uniform across the whole device. While in structure B, the current density in the QWs near the V-pit is greatly enhanced. At the joint of the last QW and the V-pit, a leakage-like current can be clearly seen. To show more details of the current distribution, the simulated current flow vectors is illustrated in Fig. 3. In structure A, as shown in Fig. 3(a), the current flows vertically through all the QWs. However, the current flow pattern in structure B is much more complicated, as shown in Fig. 3(b). In areas far away from the V-pit, the flow pattern is similar to structure A. Approaching the V-pit, the direction of the current flow in the QWs has gradually changed from vertical to horizontal. The closer to the V-pit, the stronger the horizontal current is. Figure 3(c) shows an enlarged view of the vicinity of the V-pit. In the first flat QW which is the nearest to the n-GaN layer, the current flows horizontally toward the V-pit. After entering the sidewall QWs, a part of the current flows obliquely upward and then goes into the overlying flat QWs. In the second and third QWs, the current flows horizontally away from the V-pit and gradually becomes the vertical current flowing through the QBs. In the last QW, a part of the current flows directly upward to the p-GaN layer. The rest of the current flows horizontally toward the V-pit and then turns upward to the p-GaN at its vicinity, forming a leakage-like stream.

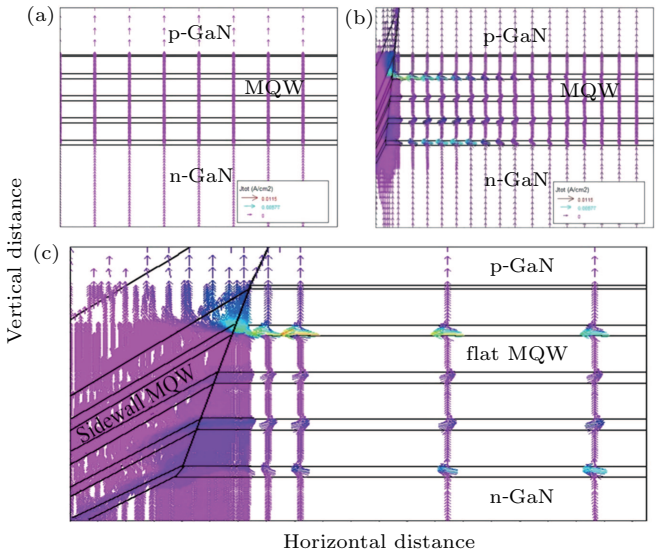



**Fig. 3.** (color online) Current flow vectors of structure A (a) and structure B (b). (c) Enlarged view of the current in the QWs.

The flow vectors in Fig. 3 have clearly shown that a considerable part of the photocurrent in structure B was transported via the V-pit sidewall. This means a large number of photo-generated carriers did not escape the QWs by directly overcoming the QBs. Instead, they escaped the flat QWs via the V-pit sidewall. To understand the carrier transport mechanism in structure B, we come up with a carrier transport model based on WKB approximation. For simplicity, we investigate the situation of electron here. According to Lang *et al.*'s work,[15] a formulation of the carrier lifetimes ($\tau$) is calculated as follows:

$$\frac{1}{\tau} = \frac{1}{\tau_{\mathrm{SRH}}} + \frac{1}{\tau_{\mathrm{T}}} + \frac{1}{\tau_{\mathrm{TE}}}, \tag{2}$$

where $\tau_{\mathrm{SRH}}$ represents the lifetimes for SRH recombination, $\tau_{\mathrm{T}}$ and $\tau_{\mathrm{TE}}$ represent the lifetimes for tunneling and thermionic

emission. The SRH lifetime is set to be 100 ns in prior discussion and the radiative recombination under zero bias is negligible, so we primarily discuss tunneling and thermionic emission of the loss mechanisms for photon - generated carriers. The tunneling probability and the thermionic emission probability from the ground state of QW is calculated as follows:

$$\frac{1}{\tau_{\mathrm{T}}} = \frac{\pi\hbar}{2L_w^2 m^*} \exp \int_0^{L_b} -2\sqrt{\frac{2m^*(E_c(x)-E_1)}{\hbar^2}}\,\mathrm{d}x, \quad (3)$$

$$\frac{1}{\tau_{TE}} = \left(\frac{\pi\hbar}{2\pi m^* L_w^2}\right)^{1/2} \exp\left(-\frac{E_{\mathrm{c\,max}}-E_1}{k_{\mathrm{B}}T}\right). \quad (4)$$

In Eqs. (3) and (4), the $L_{\mathrm{w}}$ and $L_{\mathrm{b}}$ are QW and barrier thickness, respectively, the effective masses ($m^*$) used were $0.169m_0$ for electrons. $E_{\mathrm{c}}$ and $E_{\mathrm{cmax}}$ are conduction band and the maximum potential of conduction band, respectively. $k_{\mathrm{B}}$ is Boltzmann's constant, $T$ is the absolute temperature. Figure 4 gives the schematic diagrams of electron transport. For the carriers produced in flat QW and sidewall QW, there are two ways to escape by either tunneling or thermionic emission. Some carriers produced in flat QW will overcome the energy barriers for the lateral transport to enter into sidewall QW. Both the thickness and the In concentrations are much lower compared to the flat QW region, resulting in the situation that the energy barriers for the lateral transport is much lower than vertical transport. Figures 5(a) and 5(b) show the energy band diagrams of the flat QW and the sidewall QW, while figure 5(c) shows the energy barriers for the lateral transport. The direction of the energy band tilting is related to the combination of normal built - in field and polarization - induced field, and the energy band tilting of the flat QW is even reversed. Therefore, the polarization effect for the flat QW is much lower than the sidewall region. According to the numerical results, the energy barrier of lateral transport is around 310.9 meV. The carriers overcome the lateral energy barrier by thermionic emission mechanism due to the very large thickness, resulting in the situation where the carriers are unlikely to transport through the barrier by the tunneling mechanism. Table 3 gives the tunneling and thermionic emission lifetime of the two regions (the flat region and the sidewall region) under the zero bias. When the barrier thickness is 10 nm, the lifetimes of the flat QW are much smaller than the sidewall region. In other words, it is much easier for the carriers to go through the barrier of the sidewall region than the flat region. However, not all the carriers produced in flat QW are able to cross the sidewall region because of the energy barrier of lateral transport. To study the scope of influence for the energy barrier, we change Eq. (4) into Eq. (5)

$$L = \bar{v}\tau_{\mathrm{D}}T(\Delta E) = \left(\frac{k_{\mathrm{B}}T}{2\pi m^*}\right)^{1/2} \tau_{\mathrm{D}} \exp\left(-\frac{E_{\max}-E_{\min}}{k_{\mathrm{B}}T}\right). \quad (5)$$

In Eq. (5), $T(\Delta E)$ is the possibility of thermionic emission where $\Delta E$ is the height of the energy barrier, $\bar{v}$ is the horizontal average velocity of electron, and L is the maximal length for the scope of influence of the energy barrier. In other words, the carriers which are distributed within the length can overcome the barrier and enter the sidewall. $\tau_{\mathrm{D}}$ is the lifetime of a dominant mechanism. In this case, the carriers must go across the barrier before recombination, so $\tau_{\mathrm{D}}$ is set to be $\tau_{\mathrm{srh}}$. After calculation, $L$ is around 39.1 nm. For the $In_{0.2}Ga_{0.8}N$(3 nm)/GaN(10 nm) MQW solar cell, the V-shaped pit can extract the electrons within the scope of 39.1 nm.

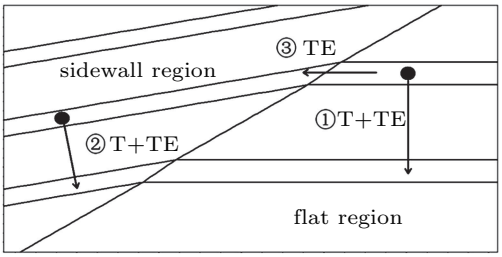



**Fig. 4.** (color online) The schematic diagrams of electron transport. ① and ② mean the carriers produced in flat QW and sidewall QW. There are two ways to escape by either tunneling or thermionic emission. Some carriers produced in flat QW will overcome the energy barriers for the lateral transport to enter sidewall QW, as noted by ③. T: tunneling, TE: thermionic emission. The black solid circles imply electrons.

**Table 2.** The tunneling and thermionic emission lifetime.

| Regions | Tunneling lifetime/s | Thermionic emission lifetime/s | SRH lifetime/s |
|---|---|---|---|
| Flat region of QW | $1.48\times10^{-6}$ | $1.94\times10^{-6}$ | $10^{-7}$ |
| Sidewall region of QW | $3.17\times10^{-15}$ | $7.95\times10^{-14}$ | $10^{-7}$ |

As has been reported by Lang *et al.*, the carrier escape efficiency in InGaN/GaN MQW is strongly dependent on the barrier thickness.[15] Here we studied the effect of V-pit on solar cells as a function of barrier thickness. We simulated five cells for structures A and B, respectively, with all the parameters fixed except for the barrier thickness. The calculated current density is shown in Fig. 6(a). When the barrier thickness is 3 nm, the current density of structure A is slightly higher than structure B. This is due to the reduced absorption area of structure B. For such a thin barrier thickness, the photogenerated carriers can easily escape the QWs by tunneling. Thus the performance of the solar cells is limited by the absorption efficiency. As the barrier thickness increases, the tunneling probability decreases exponentially. Thus, the current density of structure A drops rapidly. While for structure B, the current density drop is much slower because of the fact that the carrier is collected via the V-pit. Because the amount of carriers transported via the V-pit is determined by the horizontal thermionic emission process, it should be irrelevant to the barrier thickness. When the barrier thickness exceeds 10 nm, the tunneling probability is very low, and the horizontal thermionic emission would be the dominant carrier escape

mechanism in the flat QWs. As a result, the current density of structure B becomes irrelevant to the barrier thickness, as shown in Fig. 6(a). The current density contours for structure B with 3 nm and 15 nm barrier are given in Figs. 7(a) and 7(b), respectively. It is shown that the current distribution in MQW with 3 nm barriers is quite uniform and the horizontal current can hardly be seen. While in the cell with 15 nm barriers, the current distribution is the same as that of the cell with 10 nm barriers. It should be noted that the above discussion is based on an assumption of the same crystal quality for the MQWs with different barrier thickness. In fact, it has been demonstrated by Wierer *et al.* that a relatively thick barrier (> 6 nm) is necessary for InGaN/GaN MQW solar cell to guarantee a satisfying crystal quality.[31] Therefore, the carrier transported via V-pit should be an important factor to be considered for design of InGaN/GaN MQW solar cells.

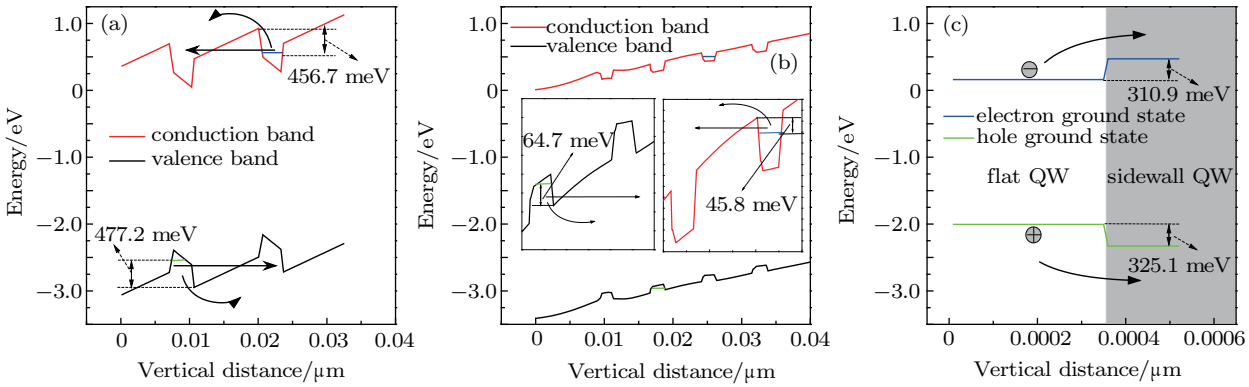



**Fig. 5.** (color online) (a) Energy barriers for carrier escaping from flat quantum well. (b) Energy barriers for carrier escaping from sidewall quantum well. (c) Energy barriers for carrier entering sidewall quantum well from flat quantum well.

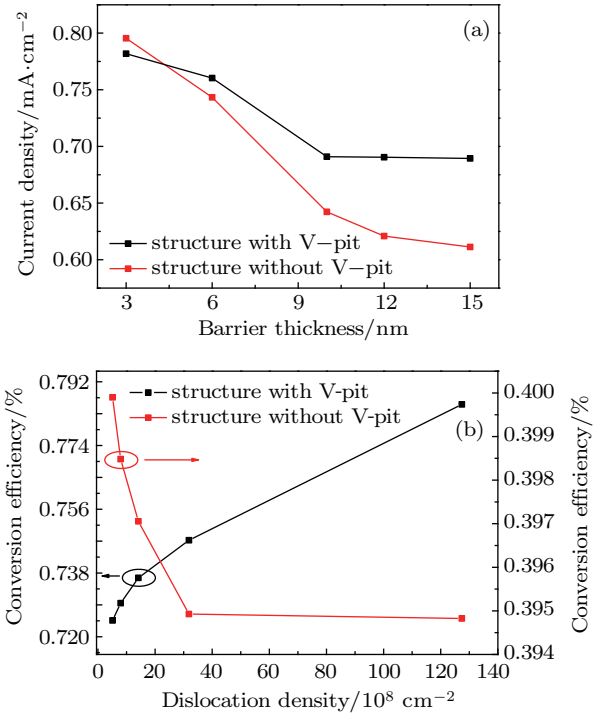



**Fig. 6.** (color online) (a) Current density as a function of barrier thickness. (b) Conversion efficiency as a function of V-pit density.

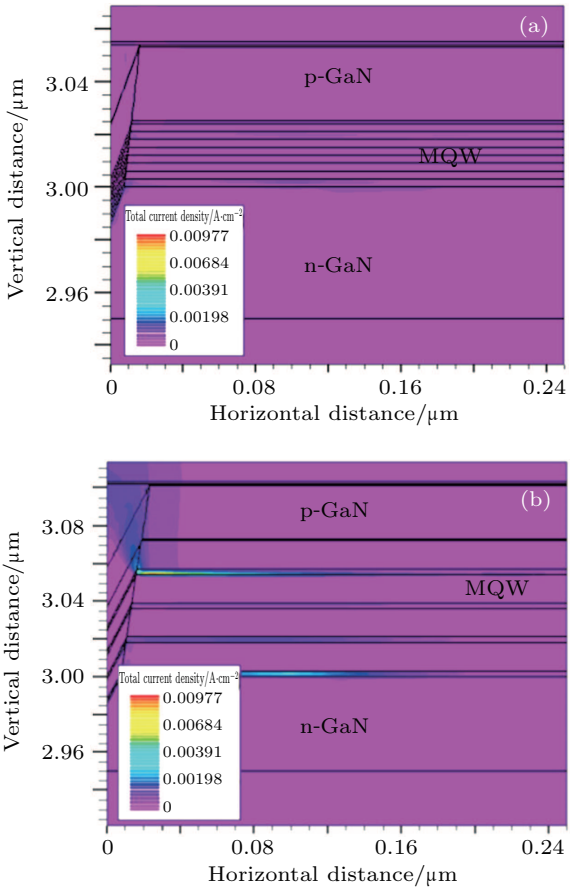



**Fig. 7.** (color online) Current density contours of structure B with (a) 3 nm barriers and (b) 15 nm barriers.

In above discussions, the dislocations are not taken into account. In reality, the density of dislocation in GaN film is typically $> 10^8$ cm$^{-2}$. Under some conditions, during the growth of InGaN/GaN MQW, the dislocations can trigger the growth of V-pits which in turn is surrounding the dislocations with their sidewalls. With the assumption that all the dislocations in structure B are surrounded by the V-pits, we studied the effect of dislocation density on the conversion efficiency.

The changing of dislocation density was realized by ad-

justing the lateral size of the cells. The barrier thickness for all the simulations was fixed to be 10 nm. The calculated efficiencies are shown in Fig. 6(b). It is clear when the dislocation density is increased from zero to $5\times10^8$ cm$^{-2}$, the efficiency of the cell without V-pit sharply decreases from 0.575% to 0.40%. This indicates that a large part of photo-generated carriers were exhausted by the NRCs of dislocation. Further increasing the dislocation density, the efficiency continues to decrease. While for the structure with a V-pit, as the dislocation density increases, the efficiency shows an increase instead of decrease. This is not surprising because the dislocations are surrounded by the V-pit sidewalls. As discussed before, the carriers entered the V-pit would be transported along the sidewall and could not reach the dislocation. In other words, the NRCs are screened by the V-pit. On the other hand, the increase of dislocation density means an increase of the V-pit density, which is beneficial to the carrier collections. Therefore, manipulating the growth of V-pits can not only eliminate the harmful effect of the dislocation but also improve the carrier collection efficiency.

## 4. Conclusions

It is revealed that the V-pits have a great influence on the carrier transport in InGaN/GaN MQW solar cells. Due to the relatively low indium composition of the MQW on the V-pit sidewall, the carriers generated near the vicinity of the V-pit can enter the V-pit and transport via the sidewall. Thus, the sidewall QWs can act as parallel escape paths for the carries generated in the flat quantum wells. For MQW with thick barrier, the carrier transport via V-pits could be dominant. Furthermore, it is found that the V-pits can reduce the recombination losses of carriers due to their screening effect to the dislocations. These discoveries are important for design of the InGaN/GaN MQW solar cells.

## References


[1] Wu J 2009 *J. Appl. Phys.* **106** 011101
[2] Bhuiyan A G, Sugita K, Hashimoto A and Yamamoto A 2012 *IEEE J. Photovolt.* **2** 276
[3] Holec D, Zhang Y, Sridhara Rao D V, Kappers M J, McAleese C and Humphreys C J 2008 *J. Appl. Phys.* **104** 123514
[4] Jani O, Ferguson I, Honsberg C and Kurtz S 2007 *Appl. Phys. Lett.* **91** 132117
[5] Dahal R, Pantha B, Li J, Lin J Y and Jiang H X 2009 *Appl. Phys. Lett.* **94** 063505
[6] Lai K Y, Lin G J, Lai Y L, Chen Y F and He J H 2010 *Appl. Phys. Lett.* **96** 081103
[7] Valduezafelip S, Mukhtarova A, Grenet L, Bougerol C, Durand C, Eymery J and Monroy E 2014 *Appl. Phys. Express* **7** 032301
[8] Choi S, Shim J, Kim D, Jeong H, Jho Y, Song Y and Lee D 2013 *Appl. Phys. Lett.* **103** 033901
[9] Redaelli L, Mukhtarova A, Valduezafelip S, Ajay A, Bougerol C, Himwas C, Faurevincent J, Durand C, Eymery J and Monroy E 2014 *Appl. Phys. Lett.* **105** 131105
[10] Dahal R, Li J, Aryal K, Lin J Y and H. X. Jiang 2010 *Appl. Phys. Lett.* **97** 073115
[11] Chen X, Zhao B J, Ren Z W, Tong J H, Wang X F, Zhuo X J, Zhang J, Li D W, Yi H X and Li S T 2013 *Chin. Phys. B* **22** 078402
[12] Liang M M, Weng G E, Zhang J Y, Cai X M, LẌ Q, Ying L Y and Zhang B P 2014 *Chin. Phys. B* **23** 054211
[13] Wu H Y, Ma Z G, Jiang Y, Wang L, Yang H J, Li Y F, Zuo P, Jia H Q, Wang W X, Zhou J M, Liu W M and Chen H 2016 *Chin. Phys. B* **25** 0117803
[14] Rajabi K, Cao W Y, Shen T H, Ji Q B, He J, Yang W, Li L, Li D, Wang Q and Hu X D 2015 *Chin. Phys. Lett.* **32** 027802
[15] Lang J R, Young N G, Farrell R M, Wu Y R and Speck J S 2012 *Appl. Phys. Lett.* **101** 181105
[16] Hangleiter A, Hitzel F, Netzel C, Fuhrmann D, Rossow U, Ade G and Hinze P 2005 *Phys. Rev. Lett.* **95** 127402
[17] Quan Z, Wang L, Zheng C, Liu J and Jiang F 2014 *J. Appl. Phys.* **116** 183107
[18] Kim J, Cho Y H, Ko D S, Li X S, Won J Y, Lee E, Park S H, Kim J Y and Kim S 2014 *Opt. Express* **22** A857
[19] Li Y, Yun F, Su X, Liu S, Ding W and Hou X 2014 *J. Appl. Phys.* **116** 123101
[20] ATLAS by SILVACO Inc., Santa Clara, CA, America
[21] Fiorentini V and Bernardini F 1999 *Phys. Rev. B* **60** 8849
[22] Sala F D, Carlo A D, Lugli P, Bernardini F, Fiorentini V, Scholz R and Jancu J 1999 *Appl. Phys. Lett.* **74** 2002
[23] Zhang H, Miller E J, Yu E T, Poblenz C and Speck J S 2004 *Appl. Phys. Lett.* **84** 4644
[24] Xia C S, Li ZM S and Sheng Y 2013 *Appl. Phys. Lett.* **103** 233505
[25] Tomiya S, Kanitani Y, Tanaka S, Ohkubo T and Hono K 2011 *Appl. Phys. Lett.* **98** 181904
[26] Wu X, Liu J, Quan Z, Xiong C, Zheng C, Zhang J, Mao Q and Jiang F 2014 *Appl. Phys. Lett.* **104** 221101
[27] Vurgaftman I, Meyer J R and Rammohan L R 2001 *J. Appl. Phys.* **89** 5815
[28] Wu J, Walukiewicz W, Yu K M, Ager J W, Haller E E, Lu H and Schaff W J 2002 *Appl. Phys. Lett.* **80** 4741
[29] Wang K, Lian C, Su N, Jena D and Timler J 2007 *Appl. Phys. Lett.* **91** 232117
[30] Zhang X, Wang X, Xiao H, Yang C, Ran J, Wang C, Hou Q and Li J 2007 *J. Phys. D* **40** 7335
[31] Wierer J J, Koleske D D and Lee S R 2012 *Appl. Phys. Lett.* **100** 111119